ADVANCED ELECTROMAGNETIC METHODS FOR AEROSPACE VEHICLES

Semiannual Progress Report
(January 1, 1991 - June 30, 1991)

by
Constantine A. Balanis
El-Budawy El-Sharawy
Shahrokh Hashemi-Yeganeh
James T. Aberle
Craig R. Birtcher

Telecommunications Research Center
College of Engineering and Applied Sciences
Arizona State University
Tempe, AZ 85287-7206

Sponsored by
Grant No. NAG-1-1082
National Aeronautics and Space Administration
Langley Research Center
Hampton, VA 23665

Contents

I. INTRODUCTION

During this period the research program addressed the following three topics:

1. Composite Materials
2. Precipitation Static (P-Static)
3. Antenna Technology

On the topic of Composite Materials our main efforts were directed toward making measurements on several new samples of composite materials made available to ASU by Stanford Research Institute (SRI) through the efforts of Mr. Frank Casler of AVRADA. These samples can be classified into three distinct materials with each material having its own distinct electrical properties. In addition, attempts were made to make predictions of the effects on antenna patterns by composite materials. This will take a greater emphasis in the next reporting period.

In Precipitation Static (P-Static), the main effort was devoted toward developing a Voltage Finite-Difference Time-Domain computer code to account for the voltage variation on a conducting body as the primary source of corona discharge, instead of the electric field. Due to complexities stemming from the interactions between the potentials, the fields, and current sources, the decision was made to begin with a simple two-dimensional problem without the corona discharge and check our programs in a series of simple models, culminating in the full corona discharge problem. This report deals with the first stage of such development.

During this reporting period, the main effort in Antenna Technology was toward the design, fabrication, and testing of a cavity-backed slot antenna using ferrite material. Using the ferrite material available to us during this period, the resonances of this antenna were around 5 and 8 GHz. Attempts will be made to model such an antenna and to lower its resonance down into the VHF and UHF bands.

II. COMPOSITE MATERIALS

A. Introduction

In previous reports we discussed waveguide techniques to measure material properties. Using this technique, the sample to be measured is cut to the exact inner dimensions of a rectangular waveguide. The sample is then placed in a sample holder as shown in Figure 1, and the S-parameters of the sample are measured using the HP8510B network analyzer. The measurements are processed using an HP workstation to find the conductivity and dielectric constant of the material under test. In sample preparation, special attention has to be given to:

1. Surface flatness and thickness uniformity. The error due to surface roughness or thickness nonuniformity increases as the conductivity of the material increases.

2. The sample is placed vertically in the sample holder. A small tilt can result in errors similar to those mentioned in 1.

3. Calibration of the HP 8510B network analyzer. Time-averaging is quite necessary to get an accurate calibration and make maximum use of the dynamic range of the network analyzer.

To examine the accuracy of our test setup, we measured the S-parameters of an empty sample holder. As shown in Figure 2, the sample holder doesn't contribute to insertion loss measurements and has less than -55 dB return loss. A more important test which actually determines the dynamic range of the measurements is the transmission through a metal sheet. This test shows system leakage and noise level. As shown in Figure 3, the measured insertion loss of a 5 mils sheet of brass was about -100 dB and was fairly flat over the bandwidth (8.2–12.4).

B. Measurements of Composite Materials

Through the efforts of Mr. Frank Cansler of ARVADA, Ft. Monmouth NJ, we received seven new samples from SRI (Stanford Research Institute) of three different materials. The first type of sample was 0.0315 in. thick

fiberglass dielectric. The measured dielectric constant of this sample is $3.8 - j0.05$ as shown in Fig. 4. The dielectric constant remained very flat over the bandwidth.

The second type of sample was 0.022 in. thick carbon impregnated fiberglass. The measured conductivity of this sample is shown in Fig. 5. The measured conductivity is about 2–2.5 kS/m at the low end of the bandwidth, decreasing to 0.5 kS/m at the high end of the bandwidth. This behavior is similar to what we found in material measurements of graphite epoxy in our previous report. The insertion loss of the sample was about -35.0 dB which was almost constant over the band. We could not identify different orientations for this material. Therefore, the measured data were processed assuming the material to be isotropic.

The third type of sample was 0.036 in. thick fiberglass with one aluminum screen on the surface. The measured insertion loss of this sample was about -20.0 dB at the low end of the bandwidth and it increased slightly to nearly -22.0 dB at the high end. The conductivity of the screen side was 300–500 S/m (see Figure 6). The conductivity increases with frequency which is consistent with our measurements included in our previous progress report. The conductivity on the opposite side was much less than the conductivity of the screen side (few tens of Siemens). Also the conductivity in both the 0° and 45° orientations was quite similar for the front aluminum screen samples.

C. Discussion

Our measurements of the new samples show that:

1. The dynamic range of the HP8510B using waveguide test set can be as high as 100 dB which compares favorably to other techniques (such as the antenna chamber measurement technique) which have less dynamic range (e.g., about 60 dB for the antenna chamber technique). In addition, the waveguide techniques requires much smaller samples and will not be hampered by edge effects of the sample (as discussed in SRI progress reports for the antenna chamber measurement technique). However, the bandwidth of the measurement is limited to the bandwidth of waveguide test set itself. The measurement bandwidth

can be increased by using coaxial test set which can be used over the entire bandwidth of the HP8510B network analyzer (45 MHz–20 GHz). At present time, such a test set is not available to us.

2. The carbon impregnated samples have better shielding than aluminum screen samples (35 dB vs. 22 dB) especially at low frequency.

3. The conductivity of carbon samples decreases with frequency where as the conductivity of aluminum screen samples increases with frequency. This makes carbon samples good for low frequency applications where as aluminum screen samples are good for lightening protection and high frequency applications. We were informed that some future materials will combine both carbon impregnation and aluminum screens for versatile applications.

D. Future Work

As discussed in our previous progress report, antenna modeling using the measured electrical properties of composites gives more accurate results than modeling the composite material by a perfect electric conductor (PEC). Since helicopter platforms include several antenna systems at UHF and VHF bands, it is necessary to measure composite material properties at low frequencies As mentioned above, a coaxial test set can be used to carry out theses measurements. If such a test set became available to us, we would use it to measure the samples which we have already received from SRI, and use the results of these measurements to model and study the effects of composite material on practical UHF and VHF antennas on helicopter surfaces.

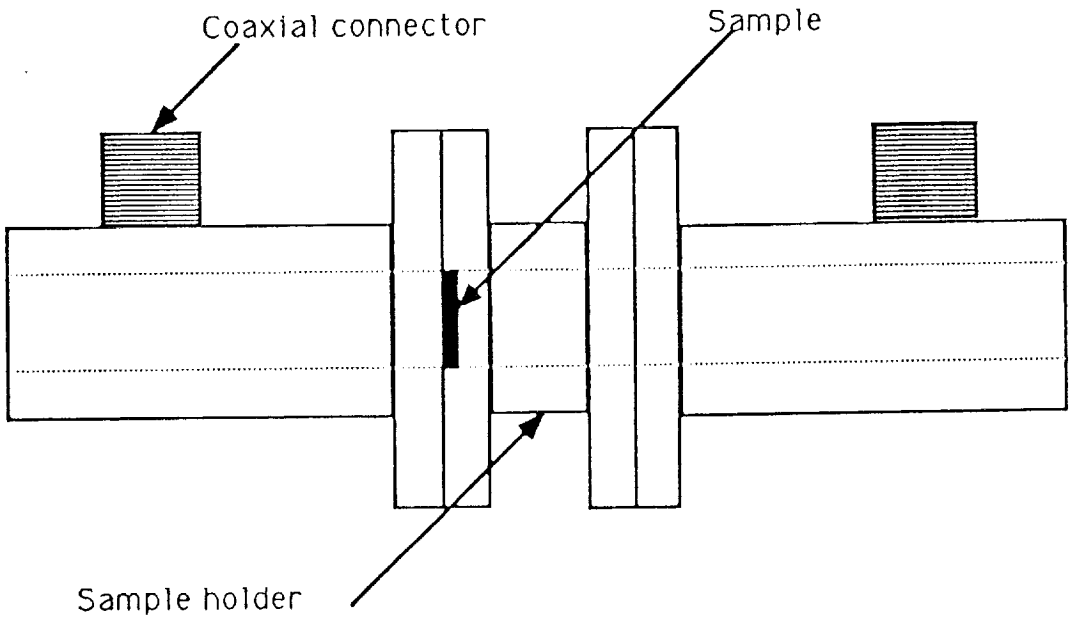

Figure 1: Geometry of the waveguide test set for material measurements.

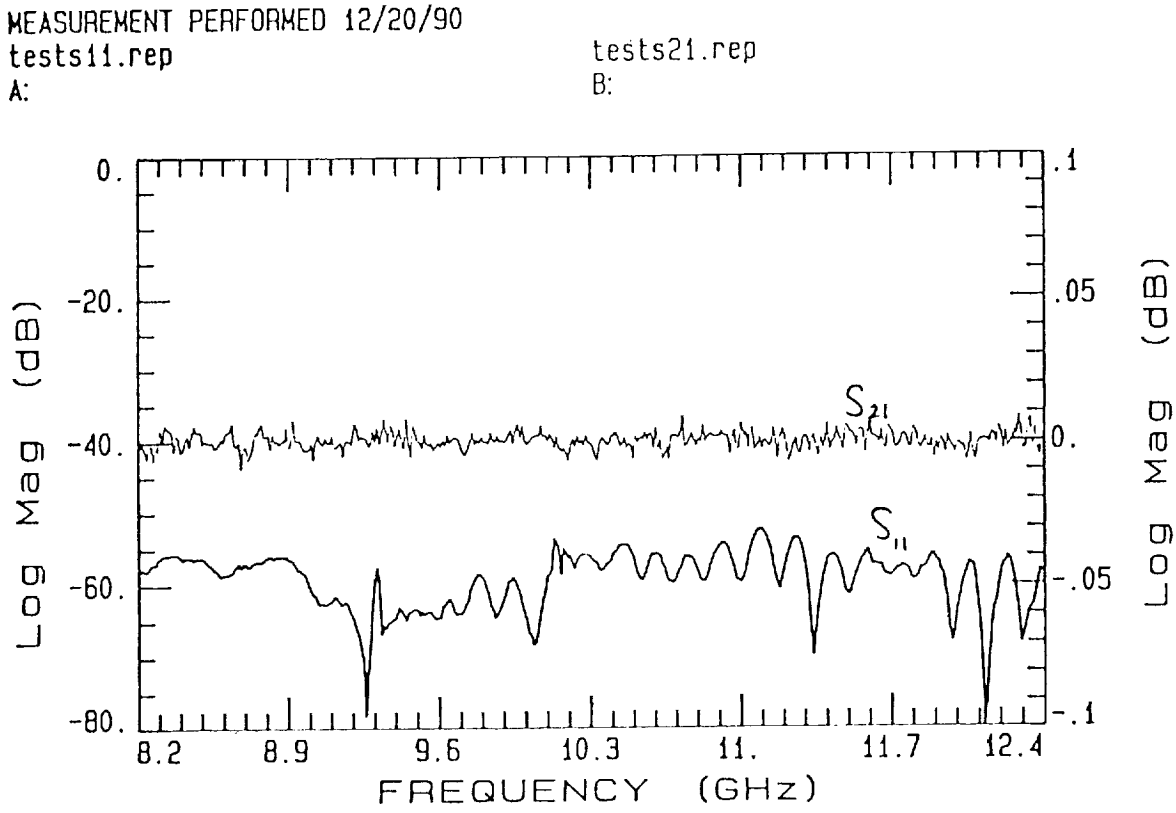

Figure 2: Measurements of the S-parameters of the sample holder.

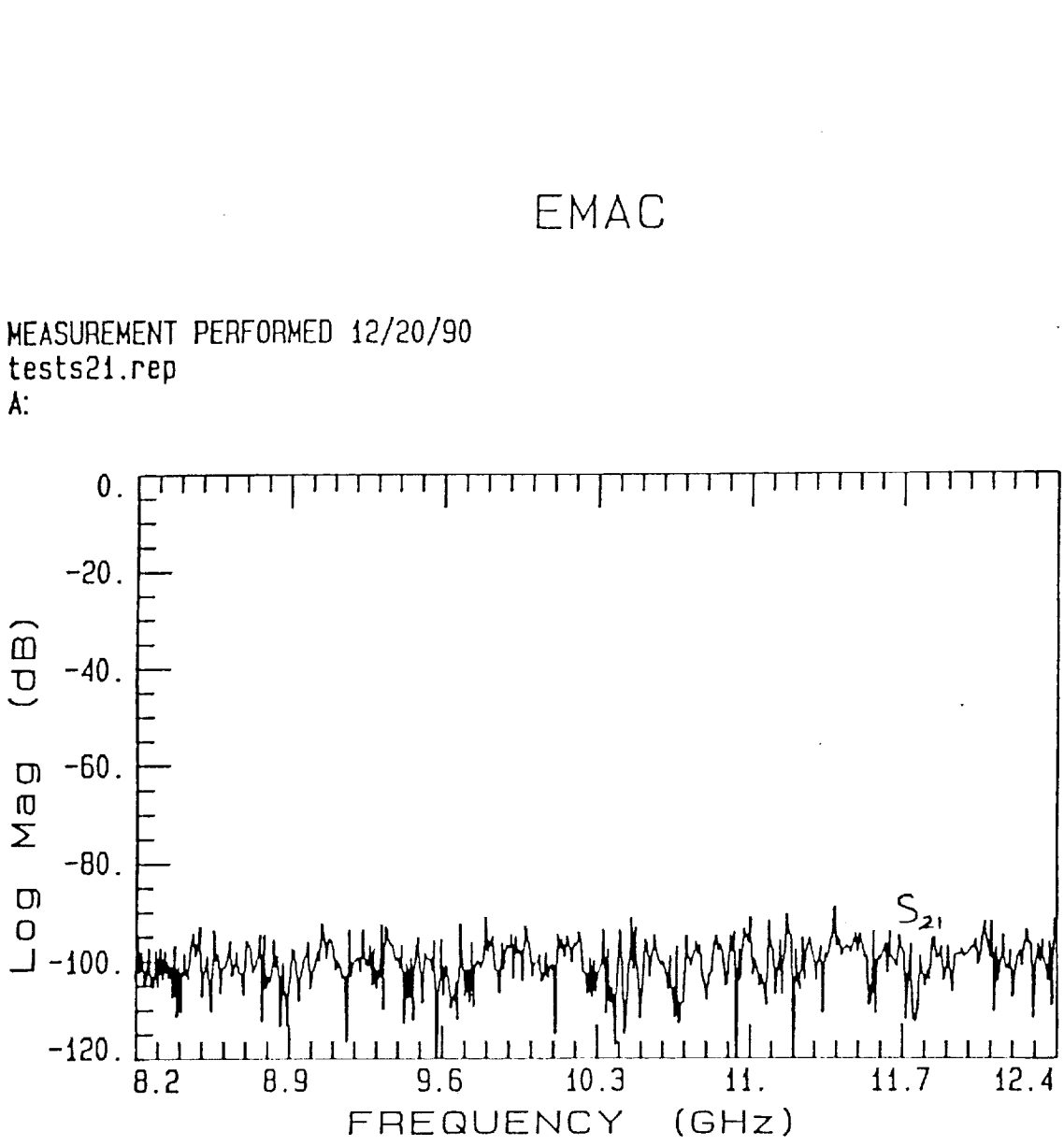

Figure 3: Measurements of the S-parameters of a brass sample.

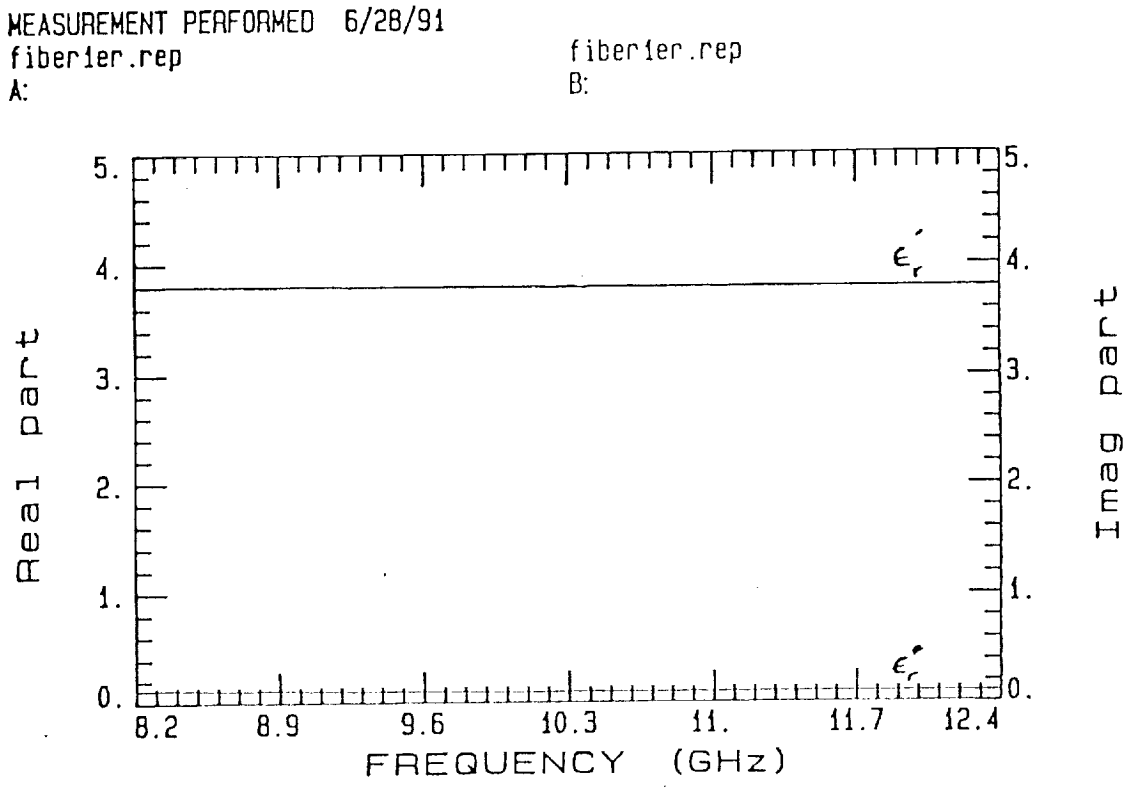

Figure 4: Measured dielectric constant of a fiberglass sample.

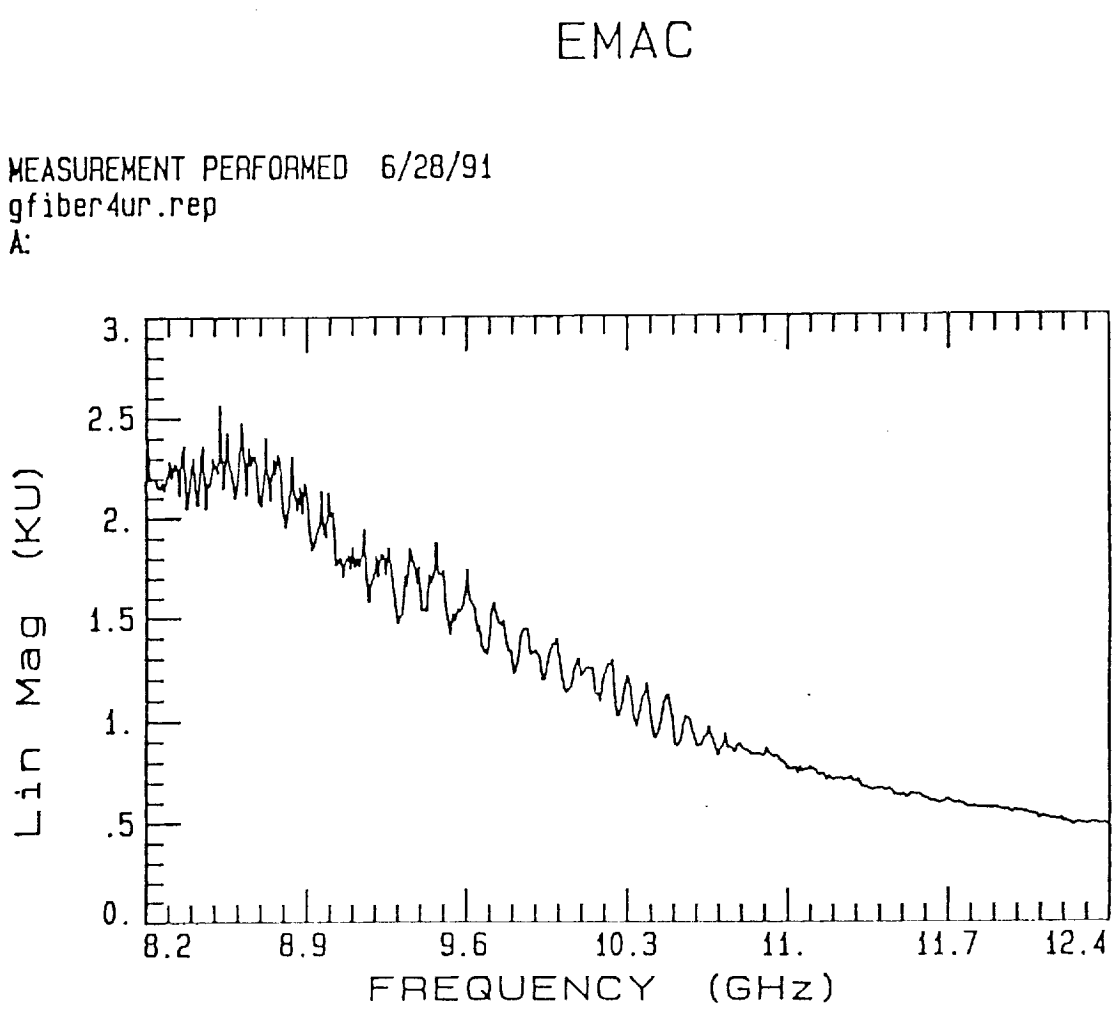

Figure 5: Conductivity of a carbon impregnated fiberglass sample.

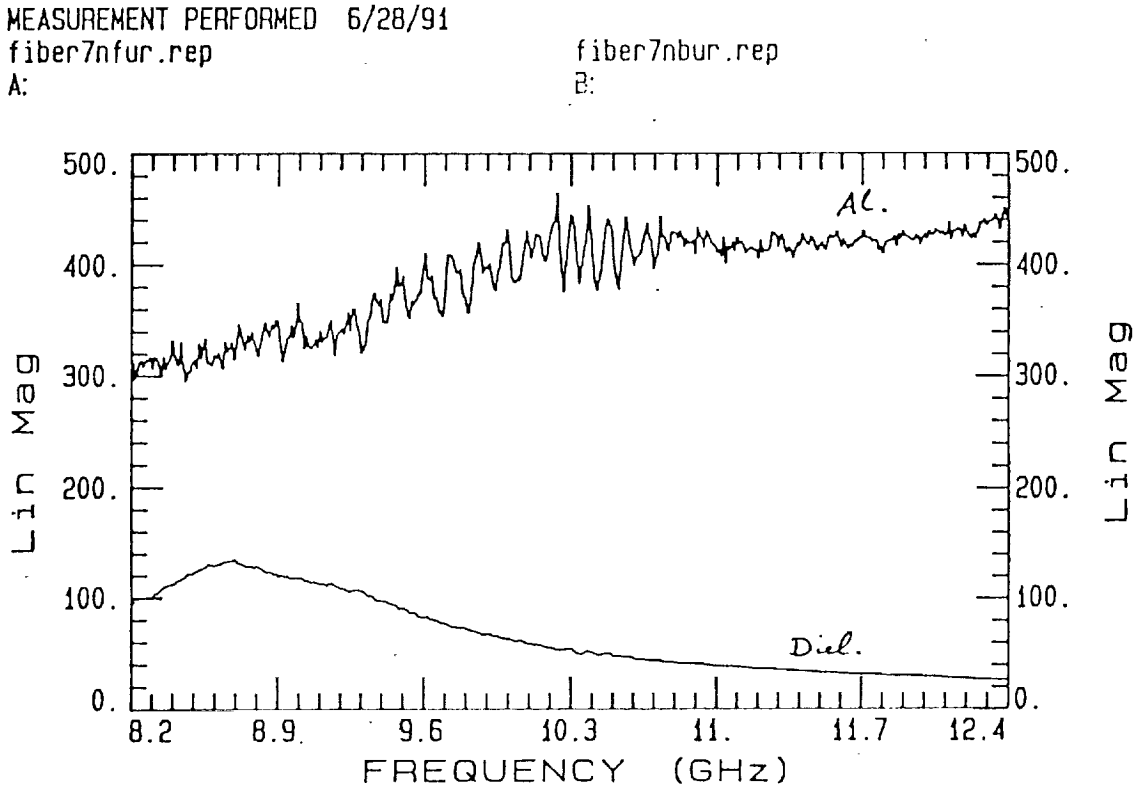

Figure 6: Conductivity of a fiberglass sample with one aluminum screen at the surface.

III. PRECIPITATION STATIC (P-STATIC)

A. Introduction

In the previous report, a new innovative method to analyze corona discharge from a highly charged conductor was proposed. In this method V the scalar electric potential, and $\vec{A}$ the vector magnetic potential were the primary unknown fields in response to any type of current source, including the corona current. Electric and magnetic fields can be found from these potentials, using the following relations:

$$\vec{E} = -\vec{\nabla}V - \frac{\partial \vec{A}}{\partial t} \tag{1}$$

and

$$\vec{B} = \vec{\nabla} \times \vec{A} \tag{2}$$

where $\vec{A}$ and V satisfy and can be derived from

$$\nabla^2 \vec{A} - \mu\epsilon \frac{\partial^2 \vec{A}}{\partial t^2} = -\mu \vec{J} \tag{3}$$

$$\nabla^2 V - \mu\epsilon \frac{\partial^2 V}{\partial t^2} = -\frac{\rho}{\epsilon} \tag{4}$$

$$\vec{\nabla} \cdot \vec{A} = -\mu\epsilon \frac{\partial V}{\partial t} \tag{5}$$

Based on the proposed method, a series of FD-TD programs are being developed for this purpose. Due to complexities stemming from the interactions between the potentials, the fields, and current sources, decision was made to begin with a simple two-dimensional problem without the corona discharge, and then to develop programs for a series of more complicated models, culminating in the full corona discharge problem. This report deals with the first stage of such development.

B. Finite-Difference Time-Domain Analysis of Non-Corona TE-Wave Microstrip Transmission Line

Consider the two-dimensional microstrip transmission line shown in Figure 7. The structure extends to infinity along the X and Z directions, while W and h are the width of the center conductor and the height of the substrate, respectively. A sinusoidal voltage source is applied between the center conductor and the ground plane to excite the potentials and fields in the substrate and the free space above the structure. To simplify the analysis at this stage, it has been assumed that the fields and potentials are Z-independent. Consequently, there is no wave propagating along Z-direction. Instead, attention has been focused on the transverse propagation of the potentials and fields. Propagation along Z-direction will be addressed in the future.

Based on this assumption, an FD-TD code has been written to compute the current on the center conductor as well as the electric and the magnetic fields at any point in space. As said before, the primary unknowns are V and $\vec{A}$ which are excited by the source voltage, and the secondary response currents on the lower and upper conductors. Figure 8 displays a flow chart that is used to develop this code. The steps in the flow chart are:

1. Step one is the initialization of the potentials, that is $V = 0$ everywhere except where the source is forced, and $\vec{A} = 0$.

2. In this step the FD-TD form of equation (1) is used to compute values of the electric field at all points. Also, these values are used to obtain the $\vec{J}_s$ and $\vec{A}$ for third step.

3. Combined FD-TD forms of equations (3) and (5) with $\vec{J} = \sigma\vec{E}$ on the conductors are used to compute $\vec{A}$ for the next iteration. Magnetic flux density $\vec{B}$ can also be determined via equation (2).

4. Electric potential values for the next iteration are computed by FD-TD form of equation (4) with $\rho_s = \vec{n} \cdot \vec{D}$ on the conductors.

Updated values of the scalar electric potentials and the vector magnetic potentials are entered back to step 2 for the next iteration. To limit the

region of the space in which V, $\vec{A}$, $\vec{E}$, and $\vec{H}$ are calculated, an absorbing boundary condition is implemented [1].

To examine the program, a structure similar to Figure 7 was simulated with $h = 0.127$ cm, $W = 3.081h$, and a relative permittivity of $\epsilon_r = 2.2$ for the substrate. The frequency of the voltage source was set at 30 GHz. The FD-TD space was divided into 32 by 32 cells. Figure 9 displays the magnitude and phase of the current distribution J_x on the strip. As it can be seen the current tends to zero near the edge. This agrees with general theoretical behavior of edge currents on a conductor. Figure 10 shows the grid point positions for some sample X-directed and Y-directed electric field components. Figure 11 displays X-directed electric field, for the four separate grid points shown in Figure 9, in time steps. It can be seen that the value of the electric field is largest close to the edge of the strip at the boundary between the substrate and free space, and it becomes smaller between the two conductors which agrees with theory. Figure 12 displays Y- directed electric field components for the four separate grid points in time steps. The values of the Y-directed electric field is highest between the two conductors and lowest outside which again agrees with theoretical prediction.

C. Conclusion and Future Work

Results based on the simplified two-dimensional Voltage Finite-Difference Time-Domain program indicate the feasibility of utilizing potentials for simulating electromagnetic problems in the cases where potentials become primary sources.

In the next reporting period, attempts will be made to implement the longitudinal propagation of the wave along the microstrip structure, and then to include a corona discharge mechanism.

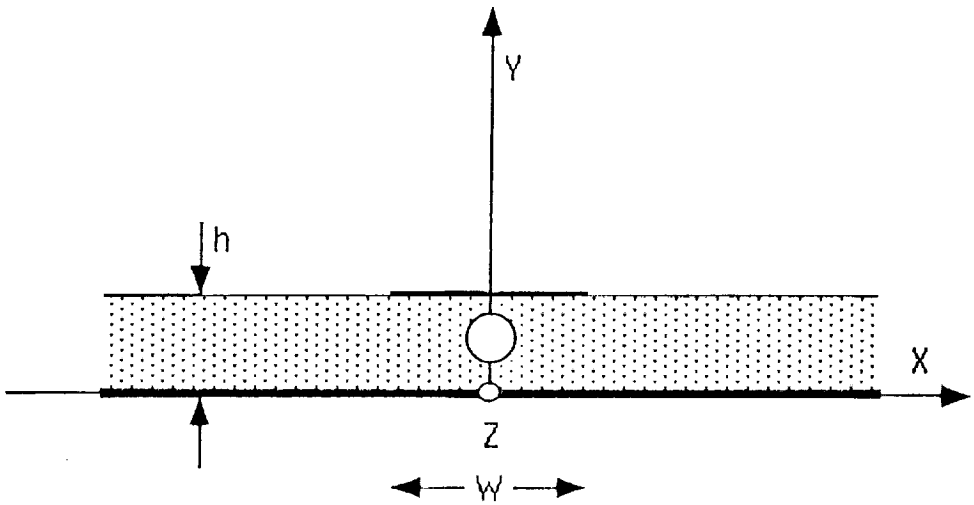

Figure 7: Microstrip transmission line excited by sinusoidal voltage source.

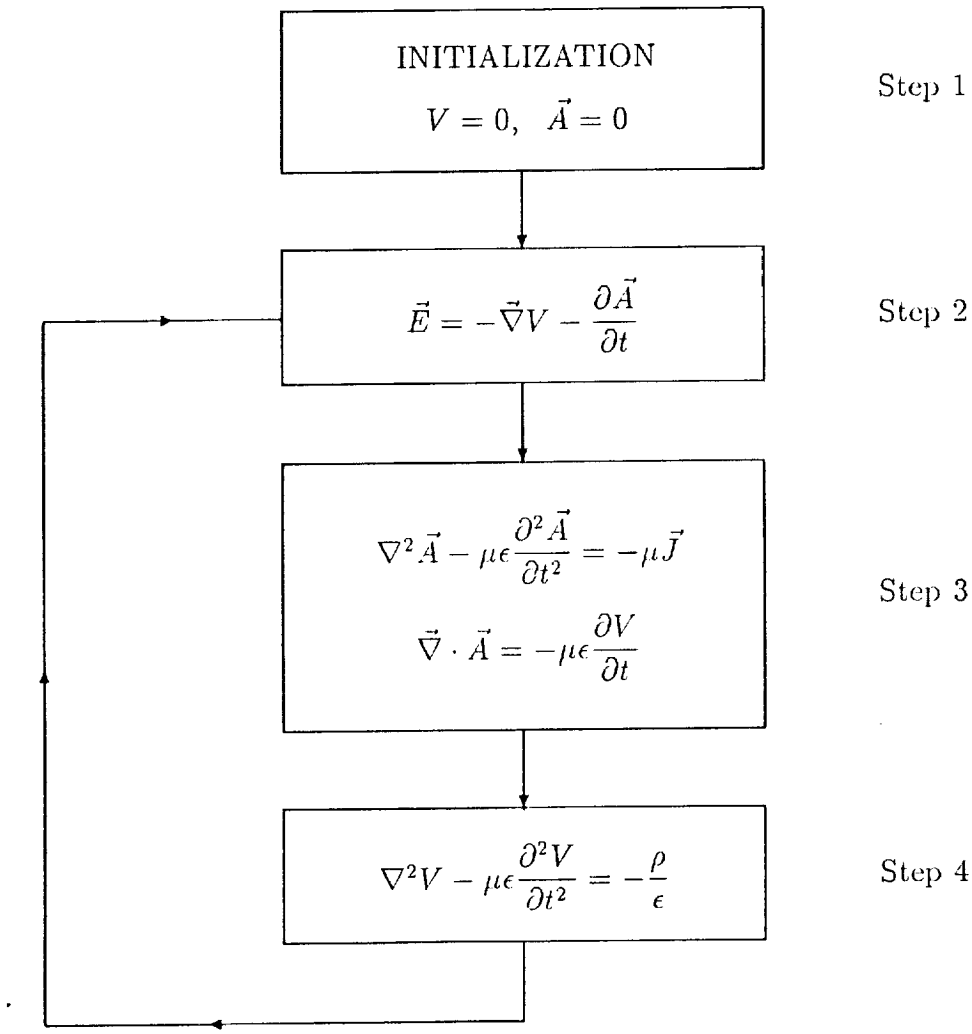

Figure 8: Flow chart for two-dimensional Voltage Finite-Difference Time-Domain analysis.

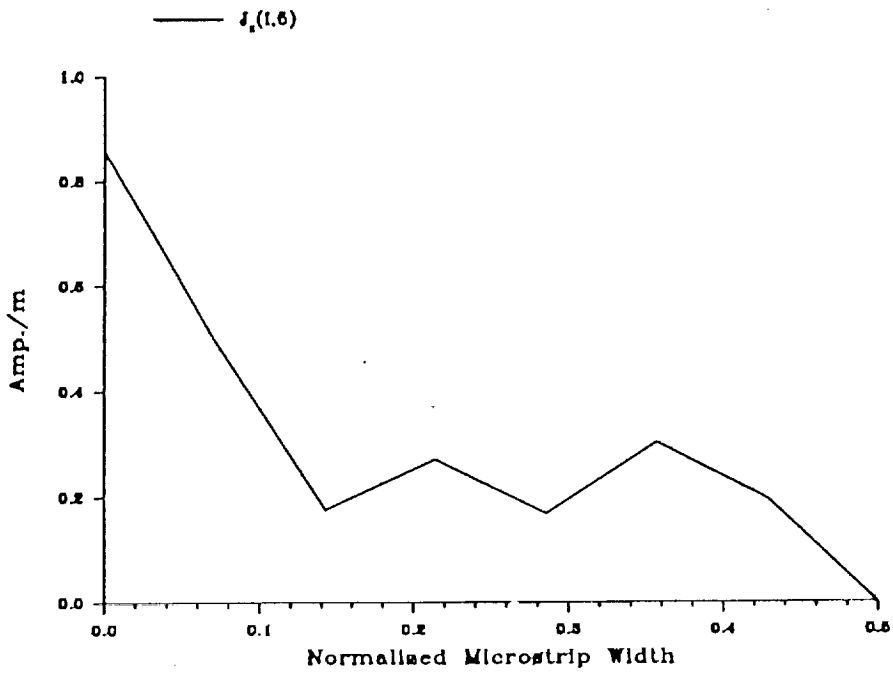

(a)

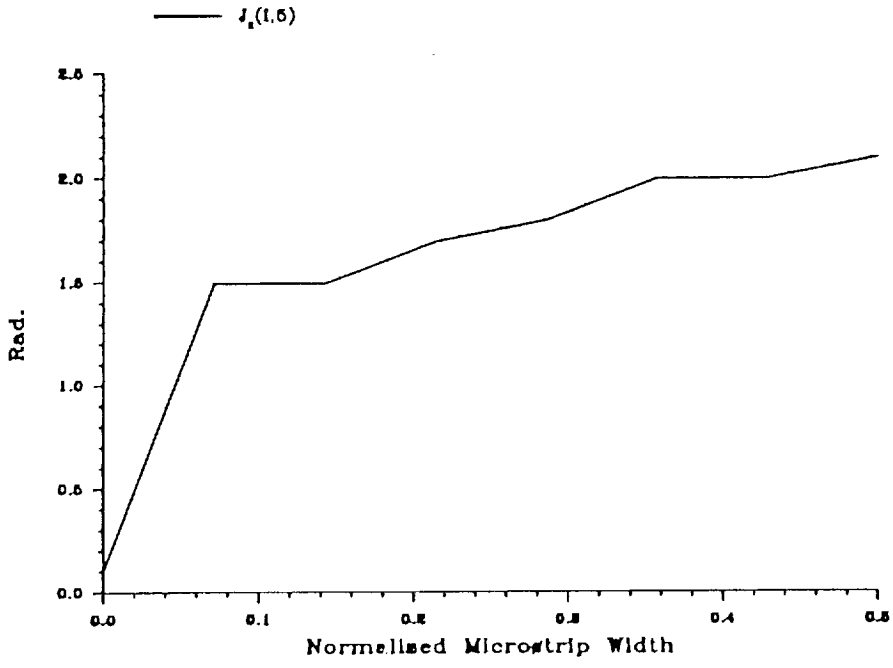

(b)

Figure 9: (a) Magnitude and (b) phase of the surface current density J_x on the center conductor.

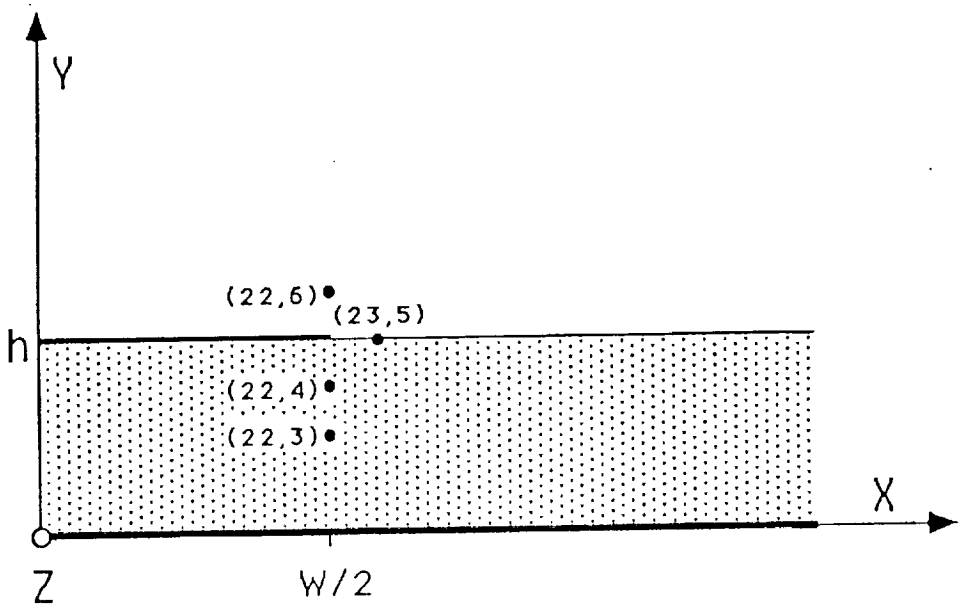

Figure 10: Grid points for sampling X-directed and Y-directed electric field components.

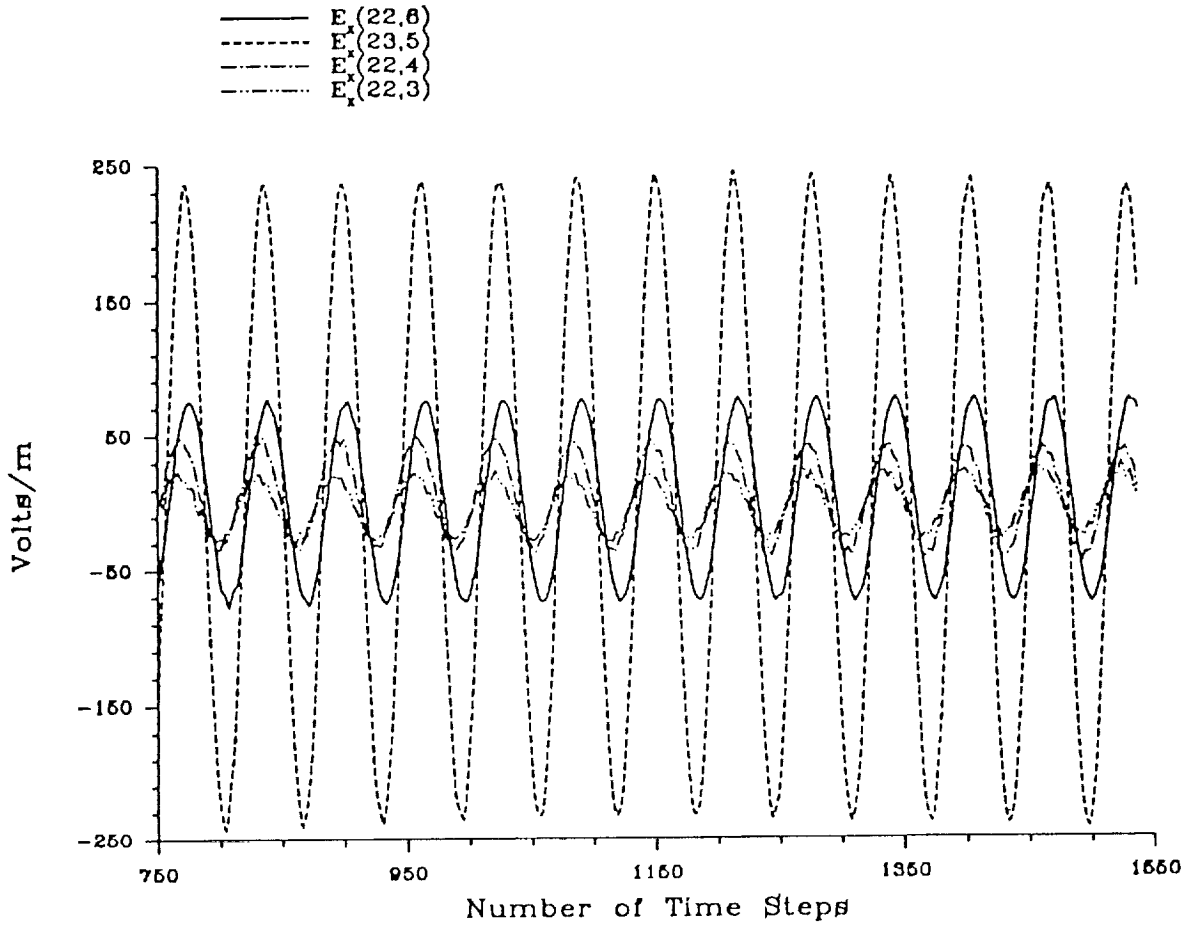

Figure 11: Values of the X-directed electric fields as function of time for four separate locations.

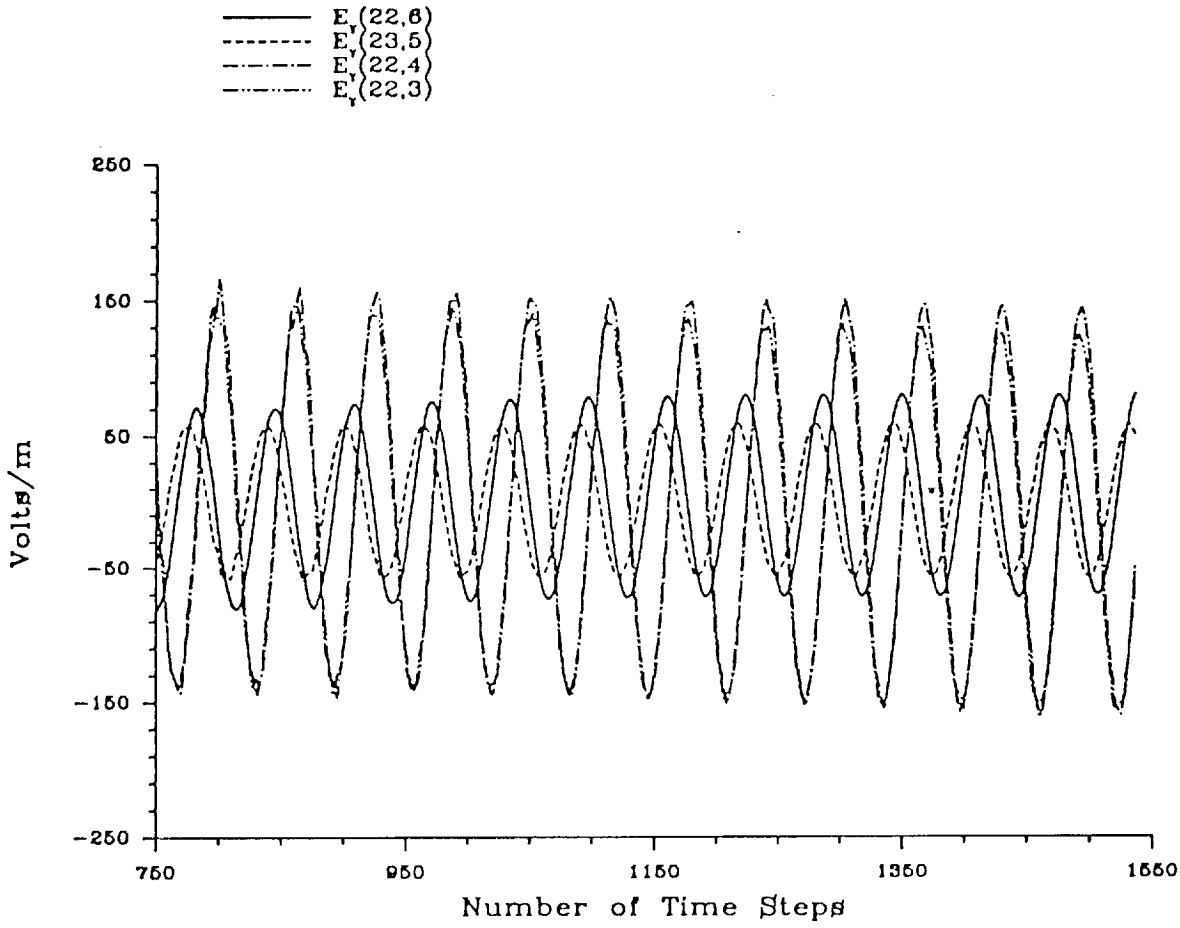

Figure 12: Values of the Y-directed electric fields as function of time for four separate locations.

S3-32

IV. ANTENNA TECHNOLOGY

A. Introduction

In this section, progress made since last quarterly report in the investigation of conformal antennas will be discussed. Two types of conformal antennas have been identified for further investigation. These are cavity-backed slot antennas and microstrip patch antennas. During the past quarter, most of our effort has been concentrated on the former.

B. Cavity Backed Slot Antenna

The objective of this work is to develop a new class of tunable flush-mounted antenna elements and arrays. These antennas comprise apertures that are backed by cavities which are partially filled with ferrite. By varying the permeability tensor of the ferrite via an applied magnetic field, the radiation and scattering responses of the antenna can be tuned over a fairly wide band.

The radiating slot is etched in the ground plane of a printed microstrip-feed network, and it is backed by a cavity that contains both ferrite and dielectric layers as shown in Figure 13. An important advantage of this feed method is its compatibility with planar MIC's such as phase shifters or amplifiers which could be placed on the feed substrate. In addition, it allows greater control of the coupling between the feed and the slot radiator. One possible disadvantage of this feed configuration is the potential for aperture blockage. Thus, we intend to evaluate the performance of a number of different feed configurations including the one shown in Figure 13.

While the primary focus of the project described above will be to exploit the tunability of the antenna, we also plan to spend some effort investigating the possibility of exploiting the non-reciprocal nature of the ferrite. For example, it may be possible to design a ferrite controlled antenna array that receives efficiently from a certain direction but does not transmit efficiently in that direction. By reversing the direction of magnetization, the transmit and receive patterns are interchanged. Because the scattering response of the antenna is proportional to the product of the receiving pattern and the transmitting pattern, the antenna is expected to have low RCS for both

magnetization states.

Cavity-backed slot antennas are widely used at microwave frequencies. However, we are investigating the possibility of using such antennas at VHF and UHF by exploiting the magnetostatic modes of the ferrite. Magnetostatic modes can have extremely high effective dielectric constant (104–105). The resonance frequency of these modes for a ferrite slab surrounded by air or dielectric layers is given by

$$f_r = \gamma \left(H_0 + \frac{4\pi M_s}{2} \right) \tag{6}$$

where $\gamma = 2.8$ GHz/kGauss, H_0 is the external magnetic field (due to the magnet) and $4\pi M_s$ is the ferrite magnetization in kGauss. It is clear that this resonant frequency will be almost independent of the physical dimensions of the cavity.

Therefore, there will be two different types of modes: the first type is dependent on the physical dimensions, dielectric constants and thicknesses of the layers filling the cavity. These modes will occur in general at higher frequencies (typically in the microwave range). The second type of modes is the magnetostatic modes which can occur at lower frequencies (VHF and UHF bands). Since magnetostatic modes are usually quite lossy, special attention has to be given to proper choice of the material (a material with narrow line width is desired) and to keeping the radiation aperture away from the ferrite material.

We have built a prototype antenna with the following dimensions and parameters:

Cavity:	0.6" × 0.4" × 0.25"
Ferrite:	$4\pi M_s = 3400$ Gauss
	$\varepsilon_r = 15.5$
	thickness = 0.025"
Dielectric:	$\varepsilon_r = 10.8$
	thickness = 0.05"

Fig. 14 shows the return loss seen by the microstrip feed line. Two resonant frequencies were observed. The first one at 5.15 GHz corresponds to the magnetostatic mode and the other resonant frequency at 8.27 GHz corresponds to the resonant frequency of the cavity.

C. Future Work

During the next quarter additional experiments on our prototype cavity-backed slot antenna will be performed. We plan to study the radiation patterns and antenna efficiency of both modes and the possibility of using other materials with much lower magnetization (we have ordered materials of $4\pi M_s = 175$ Gauss) to move the resonance to UHF and VHF regions. Also, further measurements to study the effects of external magnetic field and antenna bandwidth will soon be available. In addition to the experimental effort, computer codes to predict the performance of these antennas are under development. These codes will utilize a rigorous, fully electromagnetic approach and should provide us with a good deal of insight on how to design these antennas for optimum performance.

Also during the next quarter, we may begin to investigate various multilayer stacked microstrip antennas. By stacking microstrip antennas, one can either improve the impedance bandwidth of the antenna or increase its gain substantially.

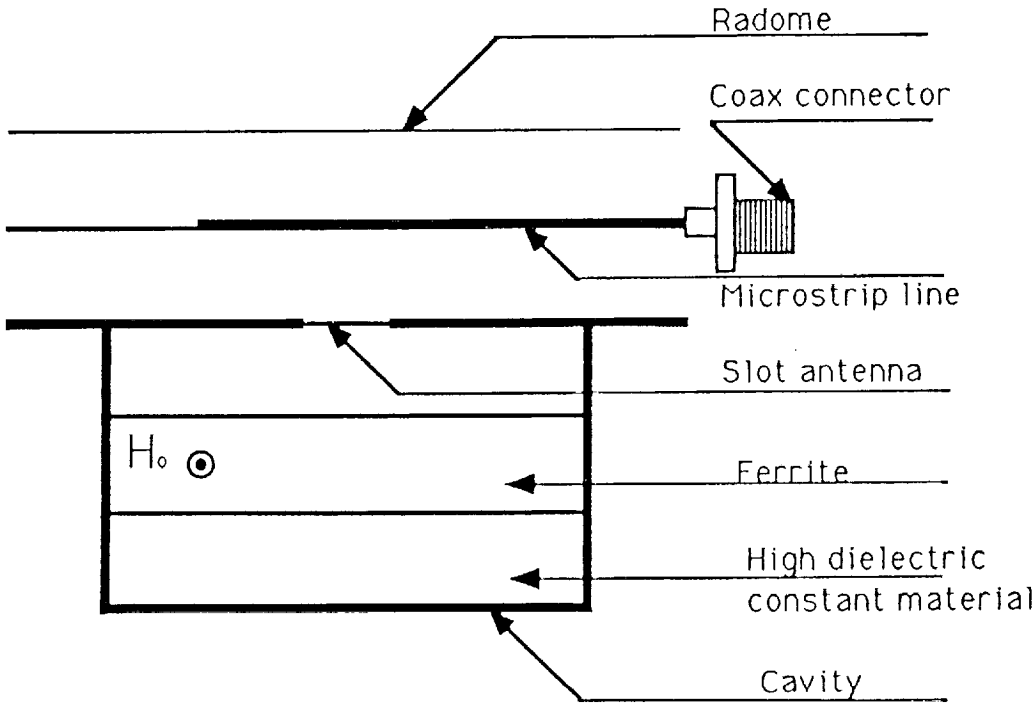

Figure 13: Geometry of the cavity-backed slot antenna.

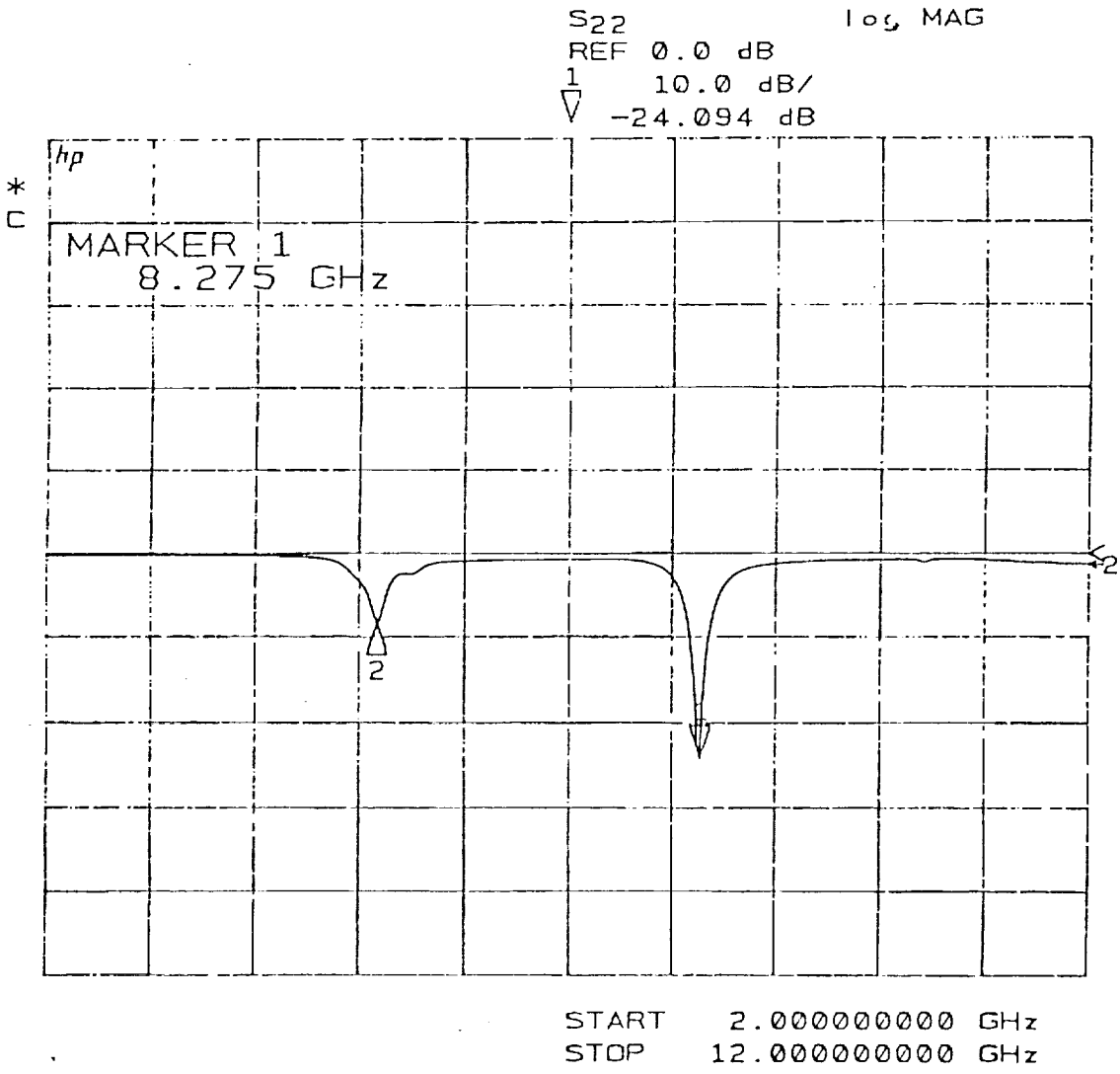

Figure 14: Measured frequency response of a cavity-backed slot antenna.

References

[1] G. Mur, "Absorbing Boundary Conditions for the Finite-Difference Approximation of the Time-Domain Electromagnetic-Field Equations," *IEEE Trans. on Electromagnetic Compatibility*, Vol. EMC-23, No. 4, pp. 377-382, November 1981.